Mechanical Behavior of Random Fiber Composite Perforated Plates

M. EGGEN, J. HAMBLETON, S. C. MANTELL AND J. DAVIDSON

ABSTRACT

In this study, the mechanical behavior of perforated, chopped fiber reinforced polymer plates is investigated. These plates serve as a manifold for polymer heat exchangers, where each perforation would be connected to a tube carrying pressurized fluid. Thus, the plates are subjected to a pressure loading. In order to predict the plate deformation due to the pressure loading, the mechanical bending behavior of these plates is quantified by an equivalent plate modulus E* and equivalent Poisson's ratio ν*, such that the perforated plate can be modeled as a solid plate. Previous research has shown that by normalizing E* with respect to the modulus of a non-perforated plate, the bending behavior of perforated plates fabricated from isotropic elastic materials was a function of the hole size, spacing and plate thickness. Machining holes in a random fiber composite creates local areas of reduced stiffness due to fiber chopping, while the previous methods used to characterize E*/E assumed uniform, isotropic material properties. The objective of this study is to demonstrate that machined chopped fiber reinforced perforated plates, which have local areas of reduced modulus near the holes, can be characterized by E*/E (an approach which assumes global isotropy). Experimental values for E*/E for non-reinforced (isotropic) and chopped fiber reinforced polymer plates are obtained for a range of hole geometries and two different polymers. These experimental results for E*/E are compared to a model developed for isotropic, elastic materials and also to a finite element solution.

1. Introduction

Compared to metal heat exchangers, polymer heat exchangers may have increased resistance to chemicals, reduced weight, and lower cost. The heat exchanger manifold is often a perforated plate which connects pressurized, fluid filled tubes together. Thus, the perforated plate is subjected to a pressure loading. Analytical and empirical models have been developed to characterize the bending

Michael Eggen, University of Minnesota, Department of Mechanical Engineering, 111 Church St. SE, Minneapolis, MN 55455

deformation of metal (or isotropic) perforated plates [1-7]. In these models, the perforated plate is characterized by an equivalent plate modulus E* and Poisson's ratio v*, such that the perforated plate can be modeled as a solid plate. These studies also showed that by non-dimensionalizing E* as the ratio E*/E, where E is the modulus of a non-perforated plate of the same material, the bending behavior of elastic isotropic perforated plates performed equally. The development of effective elastic constants allows existing analytic models for bending of solid plates to be used for perforated plates. In finite element modeling, this approach allows for perforated plates to be modeled as solid plates with the equivalent modulus and Poisson's ratio. It is unclear whether this approach can be extended to chopped fiber reinforced (FRP) perforated plastic plates.

Although random fiber composites are isotropic on a macroscopic scale, introducing holes by machining or injection molding creates local areas near the holes with moduli different from the bulk material. When constructing a perforated plate by injection molding, the material flow near the holes causes the fibers in this area to align parallel to the circumference of the hole. Thus, the process of injection molding generates an area of anisotropy, as the fiber distribution around the hole is no longer random. When introducing perforations by machining, the aspect ratios of the fibers at the edge of the hole are reduced due to fiber chopping. As predicted by the micromechanical model of Tsai and Pagano for random fiber composites, the reduced aspect ratio of the fibers at the edge of the hole will also reduce the modulus. The objective of this study is to demonstrate that machined FRP perforated plates, which have local areas of reduced stiffness near the holes, can be characterized by E*/E (an approach which assumes global isotropy). Experimental values for E*/E for non-reinforced (isotropic) and chopped fiber reinforced polymer plates are obtained for a range of hole geometries and two different polymers. These experimental results for E*/E are compared to a model developed for isotropic, elastic materials with a constant modulus throughout the plate.

2. Background

In order to understand changes that occur in the mechanical behavior of perforated plates that are constructed from FRP's, three aspects of the perforated plate problem must be considered. These aspects are the characterization of the perforated plate geometry, previous research in perforated plate deformation, and the effects of fiber chopping on the material properties of FRP's.

The four parameters that describe the geometry of a plate with an equilateral triangular perforation pattern are: pitch P, plate thickness H, hole diameter D, and web thickness h (Figure 1). The pitch is the distance between the centers of the holes, and the web thickness is the minimum thickness of the material between the holes, $h = P - D$. The amount of material removed is quantified by the dimensionless ligament efficiency μ

$$\mu = \frac{P - D}{D}. \tag{1}$$

Because material has been removed, a perforated plate will have a reduced moment of inertia and subsequently a reduced flexural modulus compared to a solid plate. Plates with an equilateral triangular hole pattern still retain isotropic elastic

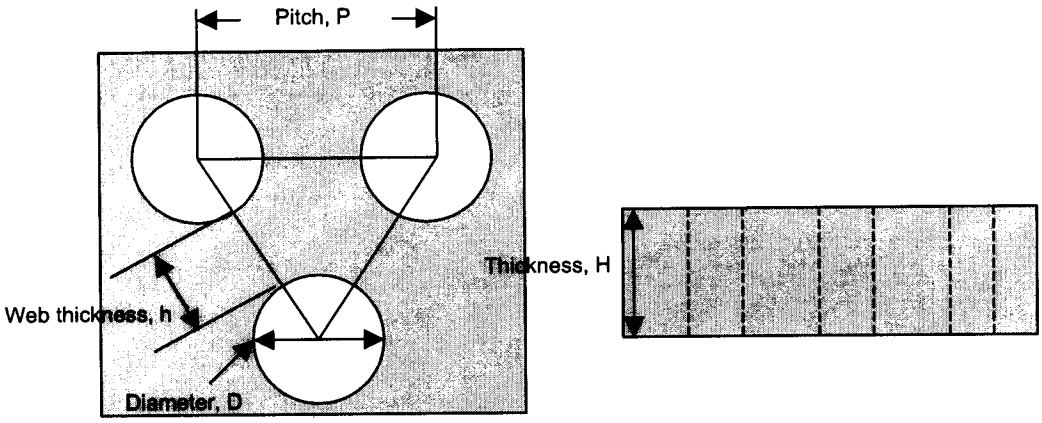

Figure 1.Top and side views of a perforated plate with an equilateral triangular hole pattern.

mechanical behavior for bending loading if the plates are constructed from a linear elastic isotropic material [1]. Thus, only two mechanical quantities are needed to characterize the bending behavior of plates with an equilateral triangular hole pattern: E^* and ν^*.

To determine these constants, both experimental and analytical methods have been employed. The experimental work includes photoelastic methods which involve polymers loaded in plane and in bending, and also four point bending tests performed with metals [1-7]. The photoelastic polymers and metals tested were linear isotropic materials. By normalizing E^* with respect to the modulus of a solid plate of the same dimensions, the experimental perforated plate results for a particular ligament efficiency can be collapsed to a single line with respect to the ratio of the plate thickness to the hole pitch (H/P).

An analytical method for quantifying the behavior of perforated plates was developed by P. Meijers [3]. This analytical model was developed for linear elastic isotropic materials by solving doubly periodic stress distribution functions for a plate. The model assumes infinite in plane plate dimensions (width and length). The model agrees well with the findings found in experimental methods and as a result, has been adopted into many pressure vessel codes. The results of Meijer's analytical model for quantifying E^*/E are shown in Figure 2 as reported by Osweiller [4]. The data are reported for values of μ=0.25 and μ=0.33, common ligament efficiencies used in heat exchanger design.

The experimental and analytical results indicate that for a fixed value of H/P, the normalized mechanical quantity E^*/E approaches 1 as μ increases (Figure 2). An increase in the ligament efficiency represents less material removal, and subsequently E^* approaches the solid plate modulus. For a fixed value of μ, E^*/E decreases rapidly from a value of 1 as H/P increases until it reaches a constant at $H/P \geq 2$. There is a transition at H/P=2 between "thin plate" behavior ($H/P<2$) and "thick plate" behavior ($H/P>2$) [2]. In plates where $H/P<2$ the stress gradient changes rapidly throughout the thickness. In plates where $H/P>2$ the stresses approach plane stress values, and E^*/E remains constant with increasing H/P. The effective Poisson's ratio ν^* depends on H/P, μ and the material property ν; however

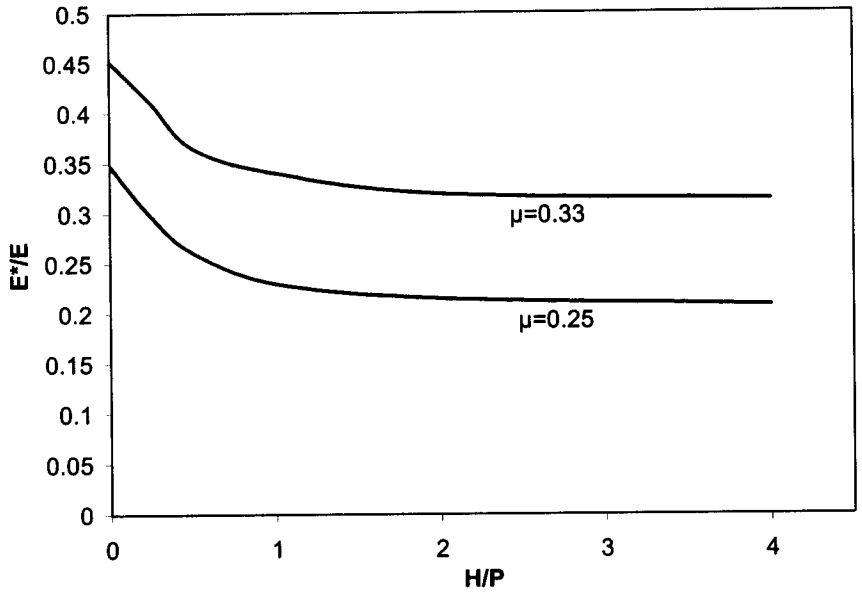

Figure 2. Meijers' analytical results for E*/E vs. H/P

ν^* has no effect on the bending modulus E*. Therefore trends in ν^* are not discussed in the present study.

The methods developed for perforated plates constructed from isotropic materials may not be valid for machined random fiber composite perforated plates. When holes are introduced by machining, a local modulus decrease is expected. At the edge of a machined hole, the average fiber length is reduced by a factor of two, as compared to the fiber length prior to machining. Thus, the average ratio of fiber length to diameter, the fiber aspect ratio, is also halved. From the Tsai and Pagano micro-mechanical model developed for random short fiber composites [8], a reduction in fiber aspect ratio creates a reduction in the composite modulus.

Tsai and Pagano related the elastic modulus E_{random} of a random short fiber composite to the corresponding oriented moduli according to the following equation:

$$E_{random} = \frac{3}{8}E_L + \frac{5}{8}E_T \tag{2}$$

where E_L and E_T are the longitudinal and transverse modulus respectively of an aligned short fiber composite having the same volume fraction of fibers. The values of the composite modulus E_L and E_T can be derived using the Halpin-Tsai micromechanical model [8]. E_L and E_T depend on the fiber aspect ratio as well as matrix and fiber stiffness and volume fractions.

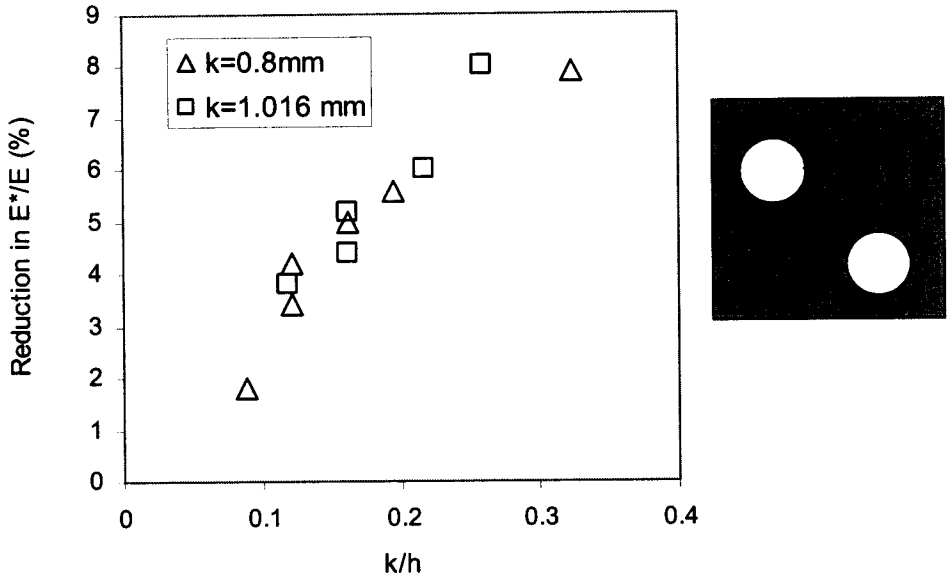

Figure 3. Finite element prediction of reduction in the normalized effective plate modulus for a local reduction of modulus of 15% near the holes, defined by k.

For a randomly oriented 30% glass fiber reinforced polyamide 6,6, a 15% reduction in modulus exists locally at the edge of a machined hole.[1] If the width of this annular region k is less than 18% of the web thickness h, then the overall normalized perforated plate modulus is reduced by less than 5% (Figure 3). One of the challenges in implementing this result is to quantify the width of the annular region affected by machining. Once this length has been identified, then the effect of the locally reduced modulus on the overall effective modulus can be discerned.

In this research, an experimental study is performed in which the hole size and spacing are varied and the effective modulus is measured. It is expected that over some range of web thickness, the normalized effective modulus E*/E will be predicted by the theory and experiments developed for perforated plates constructed from isotropic materials. As the web thickness decreases (and approaches the fiber length) the normalized effective modulus may be reduced compared to the predicted values. This reduction, if it occurs, will indicate the region near the hole, k, where a reduced modulus should be imposed.

3. Methods and Materials

The mechanical behavior E*/E for machined random fiber reinforced and non-reinforced polymer perforated plates were evaluated experimentally by three point bending. In particular, thin plates (H/P<2) with μ=0.33 were studied. The materials

[1] Assuming E_m=2 GPa, E_f=72.5 GPa [9], l/d=35, machined l/d=17.5

used were polyamide 6,6 (0% and 30% glass fiber filled) and polycarbonate (0% and 20% glass fiber filled). The values of E*/E for the reinforced and non-reinforced perforated plates for each material were compared to evaluate any effects of fiber chopping due to machining. The non-reinforced polyamide and polycarbonate plates were used for comparison as these materials represented the isotropic case. The results were also compared to the aforementioned analytical model [4].

3.1 Materials

The polyamide 6,6 (0% and 30% glass fiber filled) and polycarbonate (0% and 20% glass fiber filled) materials were purchased in 30.48cm x 60.96cm extruded sheets in thicknesses of 9.53mm and 6.35mm. The flexural moduli were found by subjecting the materials to three point bending tests in accordance with ASTM D 790-00 [10]. The flexural moduli and Poisson's ratio for these materials are listed in Table I. The uncertainty for the reinforced polymers was higher than the uncertainty for the non-reinforced polymers because of variation in moduli between individual sheets (as much as a 30% variation was found, see PA66 30% glass filled). The glass fibers in the reinforced polyamide 6,6 ranged in length from 0.432 mm to 1.016 mm with an average diameter of 0.022 mm and average fiber length of 0.762 mm as obtained with light microscopy. This yielded a range of fiber aspect ratios (fiber length/fiber diameter or l/d) from 20 to 47 with an average of 34.6. Fiber information for the reinforced polycarbonate was not obtained.

3.2 Experimental Method

Three point bending tests were performed in accordance with ASTM D 790-00 on a servo-hydraulic MTS load frame. Load data were recorded with a 2224 N (500 lb) load cell with a sampling frequency of approximately 10 Hz. For three point bend testing, the modulus of a specimen is defined as

$$E = \frac{0.25ML^3}{WH^3} \tag{3}$$

Table I. Flexural modulus and Poisson's ratio for polyamide 6,6 (0% and 30% glass fiber filled) and polycarbonate (0% and 20% glass fiber filled).

	E (GPa)	
Material	t=6.25mm	t=9.52mm
Polyamide 6,6 0% glass filled	3.48 ± 0.04	3.22 ± 0.06
Polyamide 6,6 30% glass filled	4.5 ± 0.2	4.3 ± 0.7
Polycarbonate 0% glass filled	2.56 ± 0.07	2.52 ± 0.06
Polycarbonate 20% glass filled	3.6 ± 0.2	3.6 ± 0.1

where M is the load deflection slope, L is the span length, W is the specimen width and H is the specimen thickness. The load span for the tests was 203.2mm and the span to depth ratio of the tests (L/W) was approximately four. Specimens with H=9.52 mm were deflected 2 mm at a rate of 0.14 mm/s while the specimens with H=6.25 mm were deflected 2.54 mm at a rate of 0.20 mm/s. The deflections were less than half of the thickness of the specimens to avoid nonlinearity and plastic deformation. Prior to bend testing, all specimens were dried for at least five hours at 70° C and stored with desiccates to eliminate effects of humidity on the modulus values.

Specimens were fabricated from the polyamide and polycarbonate sheets. The specimen geometries used in the experiments are listed in Table II. The geometries were selected such that standard tooling could be used to fabricate the specimens and ASTM D 790-00 would be applicable. The specimens were first cut from the extruded sheets and each tested in three point bending without perforations (geometry listed under "solid" in Table II). Then each specimen was perforated, had the width reduced, and was tested in three point bending again. To reduce the uncertainty in the modulus measurement, three point bend tests were repeated five times for each specimen configuration (solid and perforated). In this way, it was possible to assign an E*/E value to each specimen. The perforated specimens were constructed such that the perforations would not intersect the edges. The width was reduced such that the hole pattern was perfectly bisected along the longest edges of a specimen. The minimum thickness e between the edge of the outermost hole and the solid edge along the length of the thickness was

$$e = \left(\frac{\sqrt{3}}{2} P - D \right) . \tag{4}$$

Hence, for a particular plate geometry, placing two of the same specimens side by side would create one continuous hole geometry.

For a single specimen, the changes after being tested as a solid only included a reduction in width and the addition of perforations. The value of E*/E for a specimen was

$$\frac{E^*}{E} = \frac{M_p W_s}{M_s W_p} \tag{5}$$

where subscript p and s denote solid and perforated specimens.

Since there were multiple specimens at each value of H/P, the single value of E*/E reported for each material was determined by averaging the E*/E values (see equation 5) of all the specimens. Averaging the specimen values of E*/E to achieve one value of E*/E is referred to as blocking, and was preferred because of the material variability seen in the polymers. Using the blocking technique, the value of E*/E for each value of H/P was only dependent on the addition of perforations and any local areas of reduced modulus that occurred during the machining process.

Table II. Plate geometries used in experimentation.

H/P	μ	D(mm)	P(mm)	H(mm)	(W)	L(mm)	# Rows of holes	Number of specimens polyamide 6,6 0/30%		Number of specimens polycarbonate 0/20%	
0.244	0.33	17.46	26.06	6.35	45.14	304.8	2	5	6	9	9
0.335	0.33	12.7	18.96	6.35	49.25	304.8	3	4	4	9	9
0.503	0.33	12.7	18.96	9.53	49.25	304.8	3	4	4	6	6
0.67	0.33	9.53	14.22	9.53	49.25	304.8	4	5	5	0	0
0.804	0.33	7.94	11.85	9.53	51.3	304.8	5	3	3	6	6
1.34	0.33	4.76	7.11	9.53	49.17	304.8	8	0	0	6	6
solid	N/A	N/A	N/A	9.53	53.34	304.8	N/A	12	12	18	18
solid	N/A	N/A	N/A	6.35	53.34	304.8	N/A	9	10	18	18

3.3 Experimental Uncertainty

The uncertainty for the moduli reported in Table I and the experimental evaluation of E*/E was computed using the RSS (root sum of squares) method which propagates precision and bias errors [11]. The precision error is a function of the standard deviation of the data, the number of specimens used, and the student t value based on a 95% confidence interval. The bias error combines the error from individual measurements. The uncertainty in specimen geometry is the resolution in the measurement instrument. The uncertainty in the slope M (see equation 3) is half the difference between the upper and lower bounds of M based on a 95% confidence interval found by regression analysis. The uncertainty in E*/E is reported as error bars for each data point.

4. Results

4.1 Experimental Results

The values of E*/E obtained for polyamide 6,6 (0% and 30% GFR) and for polycarbonate (0% and 20% GFR) at the specified values of H/P along with the analytical solution are shown in Figure 4 and Figure 5 respectively. There was no trend in the E*/E values for fiber filled specimens falling below the values of the non-reinforced specimens. In fact, some values for the reinforced specimens exceeded that of the non-reinforced specimens. Also, for a given value of H/P, the E*/E values for the fiber filled polyamide 6,6 specimens fell within the margin of uncertainty of the non fiber filled polyamide 6,6 specimens and vice versa. Similar results were found for the specimens constructed from polycarbonate. However, for each material, fiber filled and non-fiber filled values of E*/E consistently fell below the analytical solution.

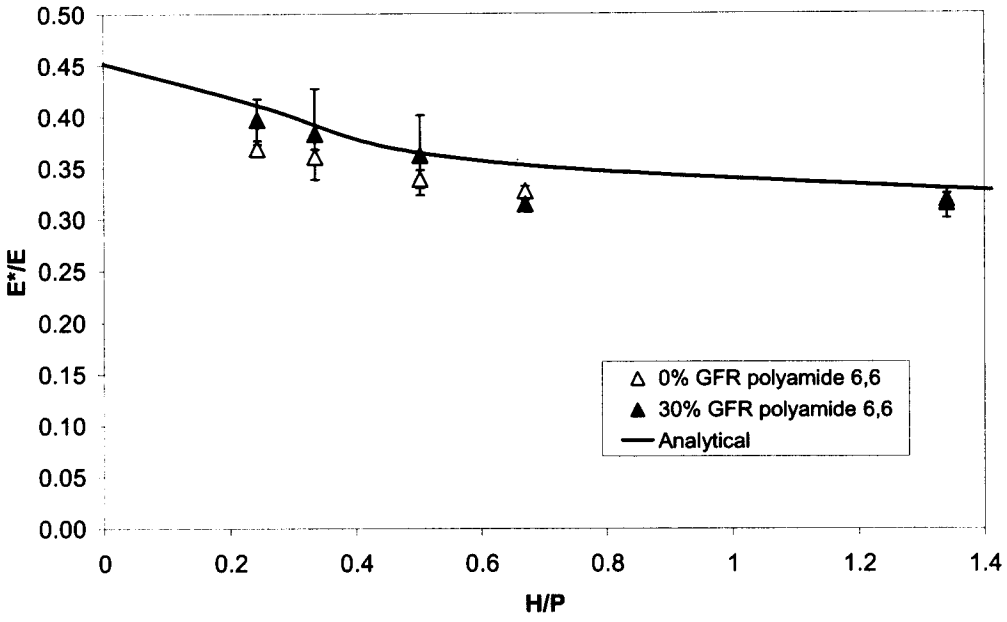

Figure 4. E*/E vs. H/P for polyamide 6,6 and 30% GFR polyamide 6,6 plotted with the analytical model.

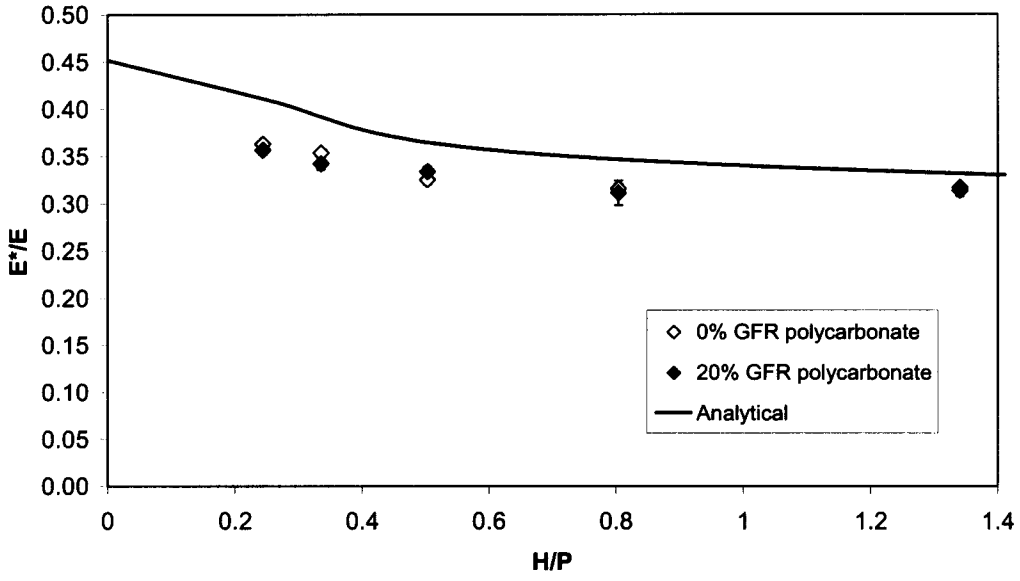

Figure 5. E*/E vs. H/P for polycarbonate and 20% GFR polycarbonate plotted with the analytical model.

5. Discussion

From the experimental results for each material, it is apparent that there is no difference in the E*/E values for chopped fiber reinforced and non-reinforced polymer plates. This outcome indicates that the width of the annular region of reduced modulus near the hole of a perforated chopped fiber specimen is small compared to the minimum web thickness of the experiment. Based on the finite element results shown in igure 3, k/h <0.1 will result in minimal effect on the effective modulus. In the present study, the minimum web thickness is 2.35 mm, thus k<0.23 mm, or approximately 1/3 of the average fiber length.

However, for each material, fiber filled and non-fiber filled values of E*/E consistently fell below the analytical solution. This difference may be the result of the plate geometry. In some instances there were only three rows of holes in the specimens, while the analytical model was developed for plates with infinite length and width. Hence, a finite element analysis was performed to determine if the experimental values that occurred agreed with a numerical analysis tailored to the specific geometry of the plates.

A 3D linear elastic analysis with an isotropic material model was performed with a commercial finite element code Abaqus (Hibbitt, Karlsson, and Sorensen) in which the stress equilibrium equations

$$\frac{\partial \sigma_{xz}}{\partial \sigma_x} + \frac{\partial \sigma_{yz}}{\partial \sigma_y} + \frac{\partial \sigma_{zz}}{\partial \sigma_z} = 0 \tag{6}$$

$$\frac{\partial \sigma_{xx}}{\partial \sigma_x} + \frac{\partial \sigma_{xy}}{\partial \sigma_y} + \frac{\partial \sigma_{xz}}{\partial \sigma_z} = 0 \tag{7}$$

$$\frac{\partial \sigma_{xy}}{\partial \sigma_x} + \frac{\partial \sigma_{yy}}{\partial \sigma_y} + \frac{\partial \sigma_{yz}}{\partial \sigma_z} = 0 \tag{8}$$

were solved simultaneously. The elements used in Abaqus were hex-dominated eight node linear bricks (C3D8R). Hex-dominated elements were used because of the increased complication in geometry encountered when modeling perforated plates. The normally brick-shaped elements change shape into a hexahedron as they encountered the holes. This feature increased accuracy due to the elements fitting the contour of the holes more closely. For a typical solid or perforated plate, 100,000 elements were used to achieve a converged solution.

The boundary conditions used in the models are shown in Figure 6. On the right face of the plate (x=L/2) an x symmetry condition was placed. Hence, on this face the x displacement $U_x=0$, rotation about the y axis $UR_y=0$, and rotation about the z axis $UR_z=0$. The use of symmetry boundary conditions reduced the number of elements in the model thereby decreasing computing time. On the left face of the plate the boundary conditions on the bottom edge were set such that $U_y=0$ and $U_z=0$. Together, these boundary conditions mimic a simply supported plate with maximum deflection δ_{max} at x=L/2.

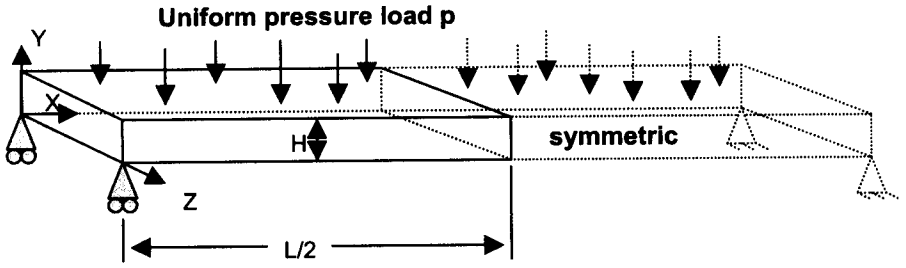

Figure 6. Loads and boundary conditions.

In the experiments, the plates were loaded by three point bending. In the finite element model, the plates were loaded in bending by imposing a uniform pressure condition on the plate surface (Figure 6). The pressure loads on the plates were chosen such that $\delta_{max}<H/2$, in order to eliminate nonlinear effects. In addition, the perforated plates with area A were loaded with a uniform pressure p such that

$$p_p A_p = p_s A_s \tag{9}$$

where subscripts s and p correspond to solid and perforated plates respectively. This ensured that both solid and perforated plates were subjected to the same total force, which simplified the calculation of E*/E. When modeling a solid plate and a perforated plate for a particular geometry, where the dimensions, material properties, and net force are equal, the quantity E*/E can be found by taking the ratio of the maximum deflection $\delta_{\max s}$ of the solid plate to that of the perforated plate $\delta_{\max p}$.

$$\frac{E^*}{E} = \frac{\delta_{\max s}}{\delta_{\max p}} \tag{10}$$

Typical polymer material properties were selected. The modulus of elasticity and Poisson's ratio used in the models were 5.8 GPa and 0.39 respectively.

The FEA values, experimental values for both materials, and the analytical model are plotted in Figure 7. The FEA values of E*/E accurately predicted the data. This result was expected because the analytical model was created for plates of infinite width and length, while the specimens in the experiments had finite geometries. The boundaries in a plate with finite geometry influence the plate performance.

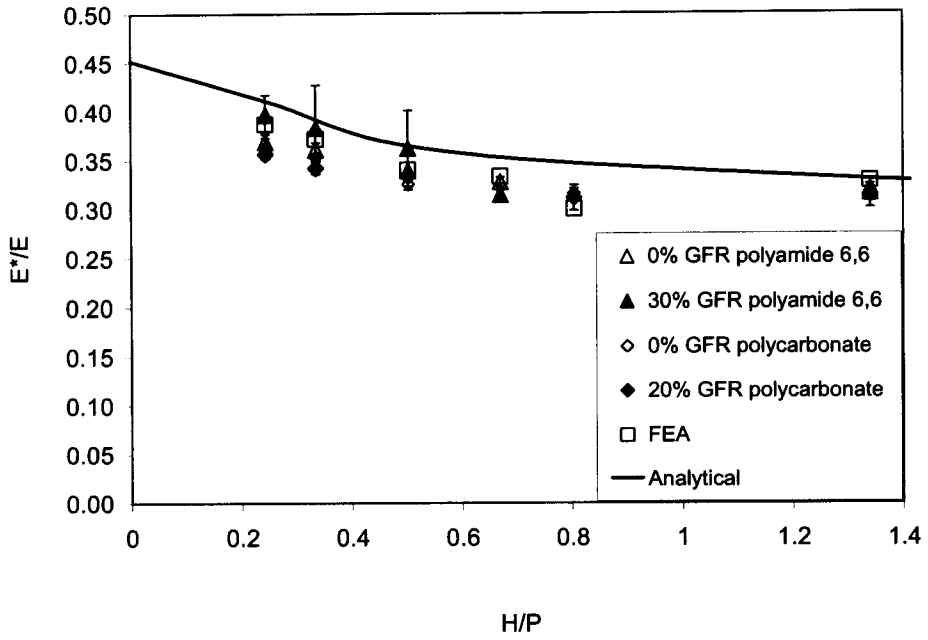

Figure 7. E*/E vs. H/P for all materials including FEA and the analytical model.

6. Conclusion

Machining holes in a random fiber composite plate reduces the fiber aspect ratio near the holes and creates local areas of reduced modulus near the holes. Assuming the fiber aspect ratio is reduced by ½, there will be a 15% reduction in modulus near the hole. In this case, for an annular region of reduced modulus with width that is less than 18% of the web thickness, the normalized effective modulus of the plate will be approximately 5% less than that predicted by previous theory developed for perforated plates constructed from isotropic, non-fiber reinforced materials. The challenge in determining the effect of machining holes in the fiber reinforced plates is to determine the size of the region of reduced modulus. In the present study, the experimental values of E*/E for fiber reinforced polymers agreed with the experimental E*/E values for the same non-fiber reinforced polymers. Thus, based on a finite element model, the region of reduced modulus near the holes has an annular width less than 1/3 the average length of the reinforcing fiber. Overall, the experimental values of E*/E, for unreinforced and reinforced plates, were less than the analytical model developed for linear elastic, isotropic materials. However, a finite element analysis was performed where the plates were modeled with a linear elastic, isotropic material and the experimental results were validated. The discrepancy occurred because of the infinite plate assumptions used to create the analytical model.

Acknowledgements:
This work was carried out in part using hardware and/or software provided by the University of Minnesota Supercomputing Institute.

References

1. Duncan, J.P., and R.R Upfold. 1963. "Equivalent Elastic Properties of Perforated Bars and Plates," Mechanical Engineering Science, 5:53-65.
2. O'Donnel, W. J., and B.F. Langer. 1962. "Design of Perforated Plates," *Journal of Engineering for Industry, 121-128.*
3. Meijers, P. 1985. "Refined Theory for Bending and Torsion of Perforated Plates," *Proceedings of the 1985 Pressure Vessel and Piping Conference, New Orleans,* 98(2):11-19.
4. Osweiller, F. 1989. "Evolution and Synthesis of the Effective Elastic Constants Concept for the Design of Tubesheets." *Journal of Pressure Vessel Technology*, 111:209-217.
5. Slot, T., and W.J. O'Donnell. 1971. "Effective Elastic Constants for Thick Perforated Plates With Square and Triangular Penetration Patterns," *Journal of Engineering for Industry,* 935-942.
6. O'Donnell, W.J. 1973. "Effective Elastic Constants for the Bending of Thin Perforated Plates With Triangular and Square Penetration Patterns," *Journal of Engineering for Industry*, 121-128.
7. O'Donnell, W.J., and B.F. Langer. 1962. "Design of Perforated Plates," *Engineering for Industry,* 307-320.
8. Biagiotti, J., S. Fiori, L. Torre, M.A. Lopez-Manchado, and J.M. Kenny. 2004. "Mechanical Properties of Polypropylene Matrix Composites Reinforced With Natural Fibers: A Statistical Approach," *Polymer Composites,* 25(1):26-36
9. Daniel, I.D. and O. Ishai. 1994. *Engineering Mechanics of Composite Materials*. Oxford University Press, Inc., pp. 28
10. ASTM D-790 - 00, "Standard Test Method for Flexural Properties of Unreinforced and Reinforced Plastics and Electrical Insulating Materials," ASTM International.
11. Beckwith, T. R. Marangoni, and J. Lienhard. 1995. *Mechanical Measurements.* Addison-Wesley, pp. 54.

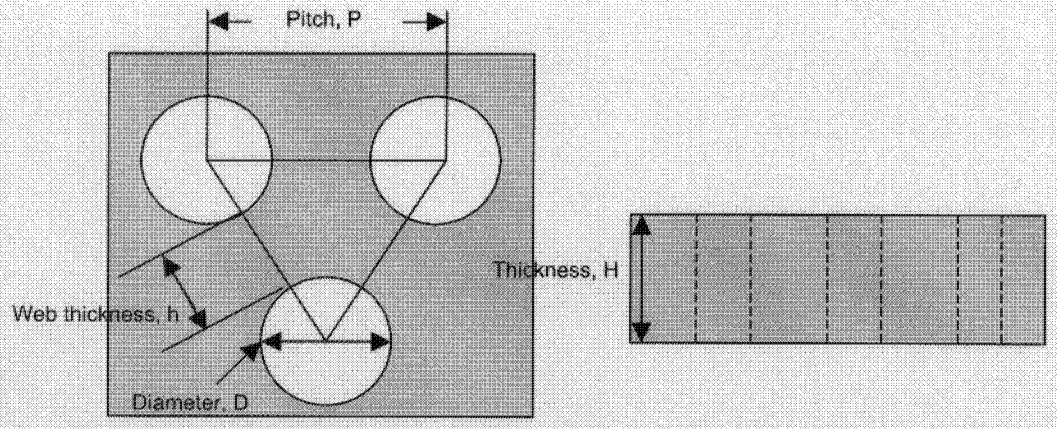

Figure 1.Top and side views of a perforated plate with an equilateral triangular hole pattern.

mechanical behavior for bending loading if the plates are constructed from a linear elastic isotropic material [1]. Thus, only two mechanical quantities are needed to characterize the bending behavior of plates with an equilateral triangular hole pattern: E^* and ν^*.

To determine these constants, both experimental and analytical methods have been employed. The experimental work includes photoelastic methods which involve polymers loaded in plane and in bending, and also four point bending tests performed with metals [1-7]. The photoelastic polymers and metals tested were linear isotropic materials. By normalizing E^* with respect to the modulus of a solid plate of the same dimensions, the experimental perforated plate results for a particular ligament efficiency can be collapsed to a single line with respect to the ratio of the plate thickness to the hole pitch (H/P).

An analytical method for quantifying the behavior of perforated plates was developed by P. Meijers [3]. This analytical model was developed for linear elastic isotropic materials by solving doubly periodic stress distribution functions for a plate. The model assumes infinite in plane plate dimensions (width and length). The model agrees well with the findings found in experimental methods and as a result, has been adopted into many pressure vessel codes. The results of Meijer's analytical model for quantifying E^*/E are shown in Figure 2 as reported by Osweiller [4]. The data are reported for values of μ=0.25 and μ=0.33, common ligament efficiencies used in heat exchanger design.

The experimental and analytical results indicate that for a fixed value of H/P, the normalized mechanical quantity E^*/E approaches 1 as μ increases (Figure 2). An increase in the ligament efficiency represents less material removal, and subsequently E^* approaches the solid plate modulus. For a fixed value of μ, E^*/E decreases rapidly from a value of 1 as H/P increases until it reaches a constant at $H/P \geq 2$. There is a transition at H/P=2 between "thin plate" behavior ($H/P<2$) and "thick plate" behavior ($H/P>2$) [2]. In plates where $H/P<2$ the stress gradient changes rapidly throughout the thickness. In plates where $H/P>2$ the stresses approach plane stress values, and E^*/E remains constant with increasing H/P. The effective Poisson's ratio ν^* depends on H/P, μ and the material property ν; however

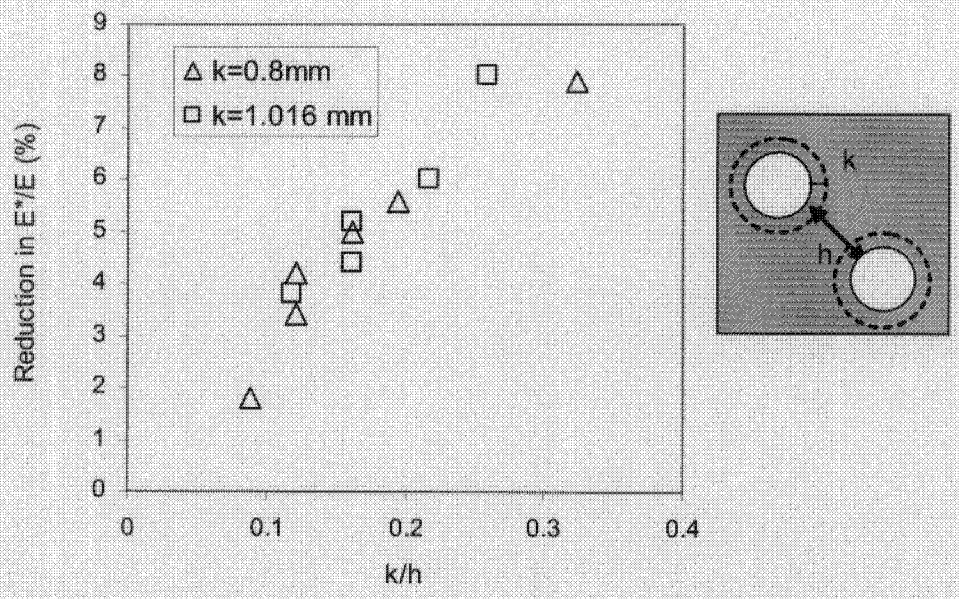

Figure 3. Finite element prediction of reduction in the normalized effective plate modulus for a local reduction of modulus of 15% near the holes, defined by k.

For a randomly oriented 30% glass fiber reinforced polyamide 6,6, a 15% reduction in modulus exists locally at the edge of a machined hole.[1] If the width of this annular region k is less than 18% of the web thickness h, then the overall normalized perforated plate modulus is reduced by less than 5% (Figure 3). One of the challenges in implementing this result is to quantify the width of the annular region affected by machining. Once this length has been identified, then the effect of the locally reduced modulus on the overall effective modulus can be discerned.

In this research, an experimental study is performed in which the hole size and spacing are varied and the effective modulus is measured. It is expected that over some range of web thickness, the normalized effective modulus E*/E will be predicted by the theory and experiments developed for perforated plates constructed from isotropic materials. As the web thickness decreases (and approaches the fiber length) the normalized effective modulus may be reduced compared to the predicted values. This reduction, if it occurs, will indicate the region near the hole, k, where a reduced modulus should be imposed.

3. Methods and Materials

The mechanical behavior E*/E for machined random fiber reinforced and non-reinforced polymer perforated plates were evaluated experimentally by three point bending. In particular, thin plates (H/P<2) with μ=0.33 were studied. The materials

[1] Assuming E_m=2 GPa, E_f =72.5 GPa [9], l/d=35, machined l/d=17.5

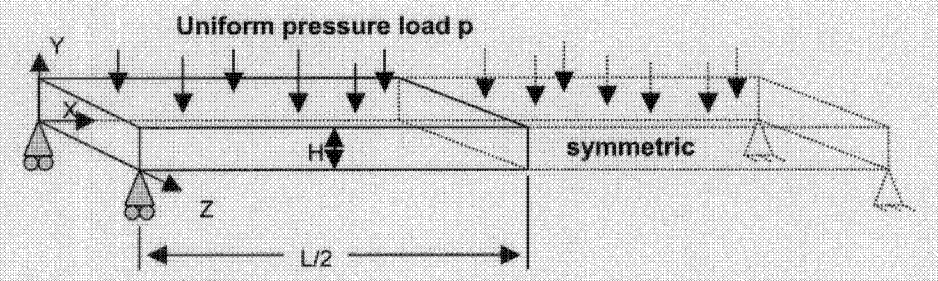

Figure 6. Loads and boundary conditions.

In the experiments, the plates were loaded by three point bending. In the finite element model, the plates were loaded in bending by imposing a uniform pressure condition on the plate surface (Figure 6). The pressure loads on the plates were chosen such that $\delta_{max}<H/2$, in order to eliminate nonlinear effects. In addition, the perforated plates with area A were loaded with a uniform pressure p such that

$$p_p A_p = p_s A_s \tag{9}$$

where subscripts s and p correspond to solid and perforated plates respectively. This ensured that both solid and perforated plates were subjected to the same total force, which simplified the calculation of E*/E. When modeling a solid plate and a perforated plate for a particular geometry, where the dimensions, material properties, and net force are equal, the quantity E*/E can be found by taking the ratio of the maximum deflection $\delta_{\max s}$ of the solid plate to that of the perforated plate $\delta_{\max p}$.

$$\frac{E^*}{E} = \frac{\delta_{\max s}}{\delta_{\max p}} \tag{10}$$

Typical polymer material properties were selected. The modulus of elasticity and Poisson's ratio used in the models were 5.8 GPa and 0.39 respectively.

The FEA values, experimental values for both materials, and the analytical model are plotted in Figure 7. The FEA values of E*/E accurately predicted the data. This result was expected because the analytical model was created for plates of infinite width and length, while the specimens in the experiments had finite geometries. The boundaries in a plate with finite geometry influence the plate performance.